Total neutron diffraction: the correct way to determine the true structure of crystalline materials?

1999 J. Phys.: Condens. Matter 11 9203

(http://iopscience.iop.org/0953-8984/11/47/307)

J. Phys.: Condens. Matter **11** (1999) 9203–9219. Printed in the UK PII: S0953-8984(99)06786-7

Total neutron diffraction: the correct way to determine the true structure of crystalline materials?

S J Hibble†, A C Hannon‡ and I D Fawcett§

† Department of Chemistry, University of Reading, Whiteknights, Reading RG6 6AD, UK
‡ ISIS Facility, Rutherford Appleton Laboratory, Chilton, Didcot, Oxon OX11 0QX, UK
§ Department of Chemistry, Rutgers University, Piscataway, NJ 08854-8087, USA

E-mail: s.j.hibble@rdg.ac.uk, a.c.hannon@rl.ac.uk and fawcett@rutchem.rutgers.edu

Received 9 August 1999

Abstract. Crystallography, using conventional Bragg diffraction, and the study of atomic correlation functions, using total diffraction, have historically been carried out separately. There exist two different scientific communities, which in the case of neutron diffraction normally use different instruments. However, modern time-of-flight neutron diffractometers allow data to be collected to high maximum momentum transfer, Q_{max}, and with good reciprocal-space resolution, $\Delta d/d$. The high Q_{max} yields correlation functions with good real-space resolution, whilst the good reciprocal-space resolution yields data well suited to conventional crystallographic analysis. We show how the Liquids and Amorphous Diffractometer, LAD, at the ISIS spallation neutron source at the Rutherford Appleton Laboratory has been used to obtain new information on a number of disordered crystalline molybdates, Li_2MoO_3, $LiMoO_2$ and D_2MoO_3. The average crystal structures are determined using Rietveld refinement of the Bragg diffraction data, whilst the local structures are determined by modelling the correlation functions, $T(r)$, obtained from total neutron diffraction data. Reconciling the information from the two techniques provides a deeper understanding of structures than is possible using either technique in isolation. Finally, we discuss how the next generation of instruments will allow the development of this technique with specific reference to the new General Materials Diffractometer, GEM, at ISIS.

1. Introduction

The identity and the structure of the basic atomic building blocks of materials are important in understanding the physics and chemistry of the solid state. The structures of crystalline materials are normally determined by fitting Bragg diffraction data using a model consisting of a unit cell and its contents, which are then repeated through space with full translational symmetry. To describe atomic positions in a fully ordered crystalline material, positional and thermal parameters are only required for the contents of one unit cell. In contrast, the structure of amorphous materials can only be completely described by models in which the atomic coordinates of every atom in the sample are specified separately, because there is no translational symmetry. At first sight this might appear to mean that the structure of amorphous materials cannot be described at as simple a level as is possible with crystalline materials, which have small units which are repeated *ad infinitum*. However, in many cases the structures of amorphous materials can also be envisaged as being made up of individual units, for example the SiO_4 tetrahedral unit, which is the basic building block in glassy silica, linked together in a non-periodic manner. Total diffraction is capable

0953-8984/99/479203+17$30.00

of producing information on internuclear distances within structural units without making assumptions about crystalline order. It can be applied to crystalline as well as amorphous materials, but this is rarely done. Structural information is obtained in the form of correlation functions calculated by Fourier transforming total x-ray or neutron diffraction data.

There are a number of notable exceptions in the literature where total diffraction studies have been carried out on disordered crystalline materials to yield information on local structure which cannot be found using conventional Bragg diffraction studies [1–8]. These studies reveal the shortcomings of conventional crystallographic analysis in which disorder is accommodated either in the temperature factors or by distributing atoms over a number of sites with fractional occupancy. In cristobalite, for example, total neutron diffraction [1–3] shows that the true Si–O bond length was significantly longer than that determined by crystallographic analysis. Soper *et al* have shown that the two different C–C bond lengths in C_{60} can be determined in the rotationally disordered phase using total neutron diffraction [4]. Total neutron diffraction has also been used to observe local metal–oxygen bond length distortions in high temperature cuprate superconductors [5], ferroelectrics [6], and more recently in the colossal magnetoresistive manganates [7, 8].

Studies of the average structure using Bragg diffraction and the local structure using total diffraction can in principle be carried out in the same experiment, although this has rarely been done [3]. We have carried out such studies using the Liquids and Amorphous Diffractometer [9] LAD, at the ISIS spallation neutron source at the Rutherford Appleton Laboratory. This time-of-flight diffractometer allows data to be collected to high Q ($\geqslant 30$ Å^{-1}), which yields good resolution in real space, and with sufficient resolution in reciprocal space ($\Delta d/d = 0.6\%$ for the backward angle detectors) for crystallographic studies.

2. Theoretical background

2.1. Total neutron diffraction

The basic quantity measured in a total neutron diffraction experiment is the differential cross section [10]

$$\frac{\mathrm{d}\sigma}{\mathrm{d}\Omega} = I(Q) = I^s(Q) + i(Q) \tag{1}$$

where $I^s(Q)$ is known as the self-scattering and $i(Q)$ is known as the distinct scattering. Q is the magnitude of the scattering vector (momentum transfer) for elastic scattering, given by

$$Q = \frac{4\pi \sin\theta}{\lambda}. \tag{2}$$

The distinct scattering is multiplied by Q to give the interference function $Qi(Q)$. For example figure 1 shows $Qi(Q)$ for Li_2MoO_3, one of the compounds discussed in this paper. The Bragg peaks are clearly visible, although the data are plotted in a way unfamiliar to a crystallographer. The interference function $Qi(Q)$ may be Fourier transformed to give the total correlation function

$$T(r) = T^0(r) + \frac{2}{\pi}\int_0^\infty Qi(Q)M(Q)\sin(rQ)\,\mathrm{d}Q \tag{3}$$

where

$$T^0(r) = 4\pi r g^0\left(\sum_i c_l \bar{b}_l\right)^2 \tag{4}$$

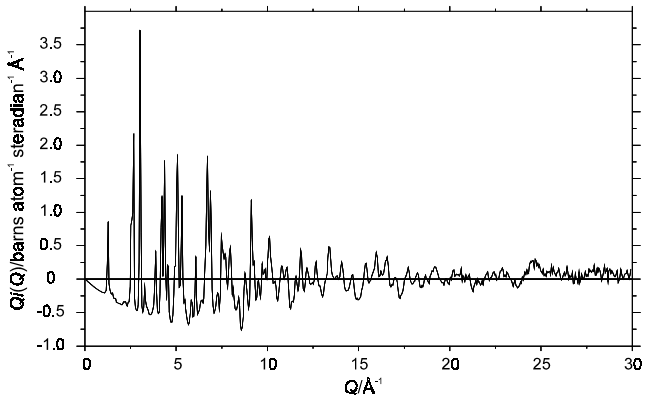

Figure 1. The interference function $Qi(Q)$ for Li_2MoO_3.

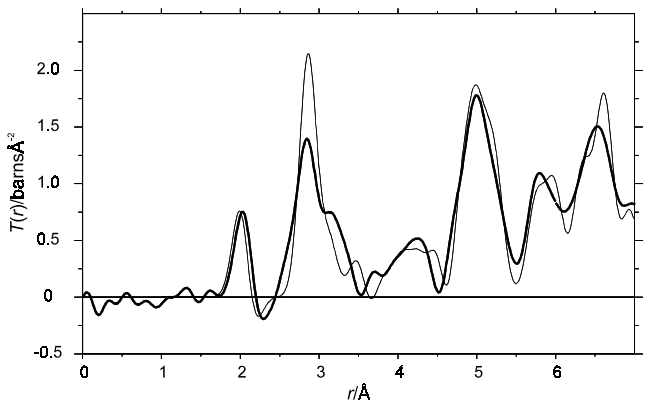

Figure 2. $T(r)_{exp}$ (bold line) and $T(r)_{model}$ calculated for the average structure from Rietveld refinement of Li_2MoO_3 (light line).

and $M(Q)$ is a modification function (used to reduce termination ripples due to the finite maximum momentum transfer, Q_{max}, of the experimental data), $g^0(= N/V)$ is the macroscopic number density of scattering units and $\bar{b}_l$ is the coherent neutron scattering length for element l for which the atomic fraction is $c_l(= N_l/N)$. The modification function used in this work is that due to Lorch [11]

$$M(Q) = \frac{\sin(Q\Delta r)}{Q\Delta r} \qquad \text{for } Q < Q_{max}$$
$$= 0 \qquad \text{for } Q > Q_{max} \tag{5}$$

where $\Delta r = \pi/Q_{max}$. Figure 2 shows $T(r)$ calculated in this way from the $Qi(Q)$ for Li_2MoO_3 shown in figure 1. The experimental total correlation function, $T(r)_{exp}$, contains information on internuclear distances. A theoretical correlation function, $T(r)_{model}$, can be calculated from a structural model, and compared with $T(r)_{exp}$, indicating how well the model describes the local structure. The model used to give the $T(r)_{model}$ in figure 2 clearly does not give a good description of the local structure in Li_2MoO_3. The origin of the model and the reasons for the discrepancies are discussed later. A numerical indication of how well $T(r)_{model}$

agrees with $T(r)_{exp}$ is given by an R-factor, defined by

$$R_{T(r)} = \left(\sum_i (T(r_i)_{exp} - T(r_i)_{model})^2 \Big/ \sum_i (T(r_i)_{exp})^2 \right)^{1/2} \tag{6}$$

where the i-summation is taken over the discrete values of r used to define $T(r)$ in the region of interest.

To calculate $T(r)_{model}$, we compute the partial pair distribution functions $g_{ll}(r)$ from the atomic coordinates and lattice parameters of the model according to

$$g_{ll'}(r) = \frac{1}{\sum_{i=1}^{N_l} w_i} \sum_{\substack{j=1 \\ j \neq j'}}^{N_l} \sum_{j'=1}^{N_{l'}} w_j w_{j'} \langle \delta(\boldsymbol{r} + \boldsymbol{R}_j - \boldsymbol{R}_{j'}) \rangle \tag{7}$$

where $\boldsymbol{R}_j$ and w_j are respectively the position and occupancy for the jth atom. The j, j' sums are over the N_l, $N_{l'}$ atoms of element l, l' and $j \neq j'$ means that j and j' are not allowed to refer to the same atom. $g_{ll'}(r)$ may be interpreted as the number density of atoms of element l' at a distance $r(= |\boldsymbol{r}|)$ from an origin atom of element l, averaged over all possible origin atoms and directions of $\boldsymbol{r}$. The weighted partial correlation functions

$$t_{ll'}(r) = 4\pi r g_{ll'}(r) \tag{8}$$

are then summed to yield the total correlation function $T(r)$

$$T(r) = \sum_{ll'} c_l \bar{b}_l \bar{b}_{l'} t_{ll'}(r) \tag{9}$$

where the l and l' summations are both over the elements of the sample. The functions $t_{ll'}(r)$ were broadened using a Gaussian function to simulate the broadening of experimental data due to thermal motion [12].

2.2. Bragg diffraction

Differential cross-section data are used in conventional Bragg diffraction studies, when the differential cross-section is treated as a function of d-spacing $d(= 2\pi/Q)$ rather than Q. The fact that Bragg diffraction can be calculated from an average unit cell and its contents, together with translational symmetry, is well known to all solid state scientists. The Rietveld method of structure refinement starts with a model with reasonable estimates of most of the atomic parameters and proceeds to improve these by least square refinement, and is well described elsewhere [13]. A numerical indication of how well the calculated and observed intensities agree may be given by the weighted profile R-factor, defined by

$$R_{wp} = \left(\sum_i w_i (Y_i(\text{obs}) - Y_i(\text{calc}))^2 \Big/ \sum_i w_i (Y_i(\text{obs}))^2 \right)^{1/2} \tag{10}$$

where w_i is the weight for point i and Y_i is the intensity of point i.

Figure 3 shows the results of a Rietveld refinement of the average structure of Li_2MoO_3. One point to note is that only a limited part of the total diffraction pattern is used for Rietveld analysis, in this case over the range $Q = 1.77$–$13.66\ \text{Å}^{-1}$ ($d = 0.46$–3.55 Å). The maximum Q (and hence minimum d) that can be used is limited because at high Q the density of reflections becomes unmanageably high. It is also worth noting that, if only Bragg diffraction is of interest, absolute normalization of differential cross-section data is not essential, because a scale factor can be used during structure refinement. For total diffraction studies absolute normalization is essential if accurate coordination number information is to be determined.

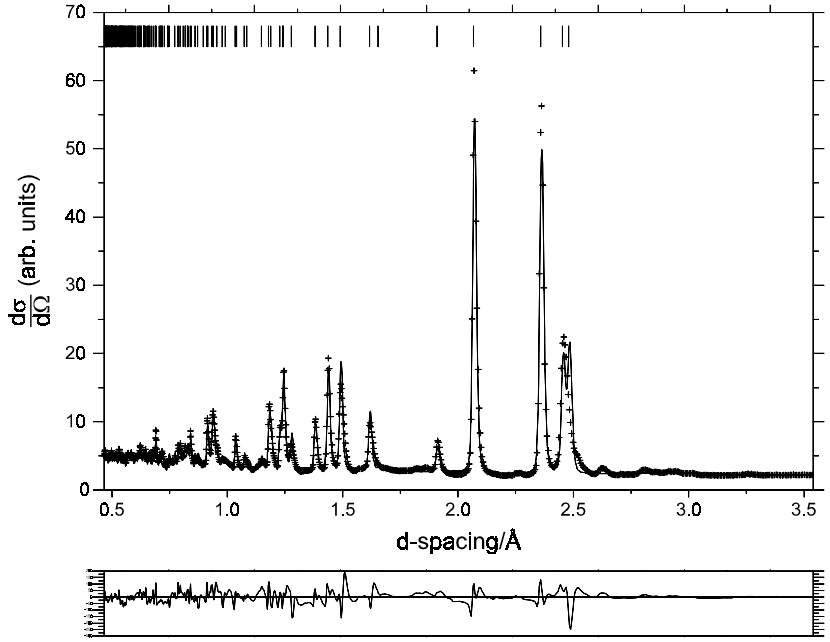

Figure 3. A neutron diffraction Rietveld profile refinement of the average structure of Li_2MoO_3. Observed data are indicated by crosses and calculated data by a solid line. Marks directly above the pattern indicate the positions of reflections. A difference curve appears at the bottom.

3. Case studies

We show here how total neutron diffraction studies can yield unique insights into the structure of disordered crystalline molybdates. In these studies the average structure is determined by conventional Bragg diffraction analysis, and the true local structure is determined by Fourier transformation of the total diffraction data to yield the total correlation function, $T(r)$. These materials exhibit a number of types of disorder, which had previously led to the publication of incorrect structures in which the structural units were not correctly described.

3.1. The lithium molybdates Li_2MoO_3 and $LiMoO_2$

The compounds Li_2MoO_3 and $LiMoO_2$ have closely related layer structures, both of which are made of MO_6 (where M is a metal atom) octahedra sharing vertices to form MO_2 layers with lithium atoms between the layers as shown in figure 4. In the case of $LiMoO_2$ all the metal (M) sites in the MO_6 octahedra shown in figure 4 are occupied by molybdenum atoms. In Li_2MoO_3 two thirds of the M sites are occupied by molybdenum atoms and one third by lithium. Rewriting the formula of Li_2MoO_3 as $Li[Li_{1/3}Mo_{2/3}]O_2$ makes the close relationship between the compounds clearer.

The precise location of molybdenum and oxygen within the MO_2 layers is of interest to condensed matter scientists concerned with the structure and properties of these materials. James and Goodenough [14] refined the average structure of Li_2MoO_3 using Rietveld analysis. Their published structure in space group $R\bar{3}m$ gave six identical M–M distances of 2.88 Å in the $[Li_{1/3}Mo_{2/3}]O_2$ layer. This disagrees with chemical and physical intuition, based on knowledge of related materials, which would suggest that the molybdenum atoms, in oxidation state IV and

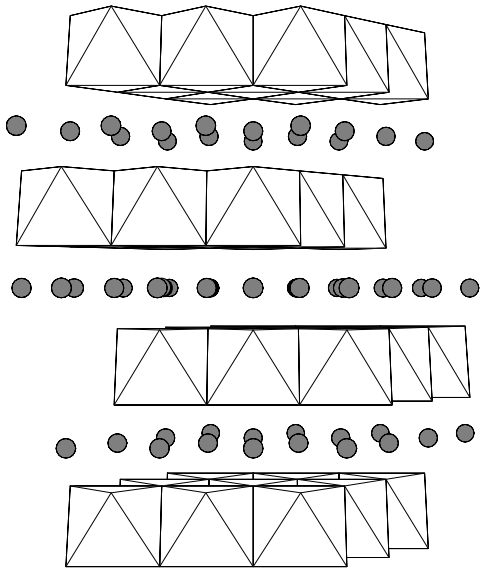

Figure 4. The layer structure of Li_2MoO_3 and $LiMoO_2$: the octahedra represent the MO_2 layers and solid, shaded circles denote interlayer lithium atoms.

with an outer electronic configuration of $4d^2$, will form metal–metal bonded triangular units. The formation of Mo–Mo bonded triangles in Mo^{IV}-containing compounds is well known, and the Mo_3O_{13} unit (figure 5(a)) is a common structural building block. So confident were James and Goodenough that these units would be found in Li_2MoO_3 that they drew Mo–Mo bonded triangles on their structural diagram even though they had not found the short Mo–Mo contacts of 2.6 Å expected for such units, see figure 5(b), in their crystallographic study. Aleandri and McCarley [15] carried out a Rietveld study of $LiMoO_2$, also in space group $R\bar{3}m$, yielding a structure with six identical Mo–Mo distances of 2.87 Å in the MoO_2 layers. They commented that this was a surprising result! In $LiMoO_2$, molybdenum is in oxidation state III with an outer electronic configuration of $4d^3$, and it would be expected to form metal–metal bonds with a bond length of about 2.6 Å. We were able to show from extended x-ray fine structure (EXAFS) measurements that it was likely that Li_2MoO_3 did indeed contain Mo_3 metal–metal bonded triangles and that the six shortest Mo–Mo bonds in $LiMoO_2$ were not identical [16]. However, it was not possible, using EXAFS alone, to determine either the true metal–metal bonding pattern in $LiMoO_2$, or the complete details of the local structure in Li_2MoO_3. We therefore turned to total neutron diffraction, using the LAD diffractometer at ISIS, to gain further information on these problems.

3.1.1. The structure of the lithium molybdate Li_2MoO_3. Unsurprisingly, our Rietveld refinement of the Bragg diffraction data for Li_2MoO_3 [17] (see figure 3) yielded results in good agreement with James and Goodenough [14], and once again a physically unreasonable structure with no evidence for Mo_3 clusters. More revealing was a comparison of the total correlation function, $T(r)$, calculated from our Rietveld model with that obtained from the total diffraction data, as shown in figure 2. This comparison clearly showed that, although the Rietveld modelling led to a reasonable reliability factor for the weighted profile, $R_{wp} = 0.1017$, the model is very poor at describing short and medium range order. The R-factor for the $T(r)$ comparison is $R_{T(r)} = 0.300$ (over the range 1.5–7.0 Å). This demonstrates a simple but

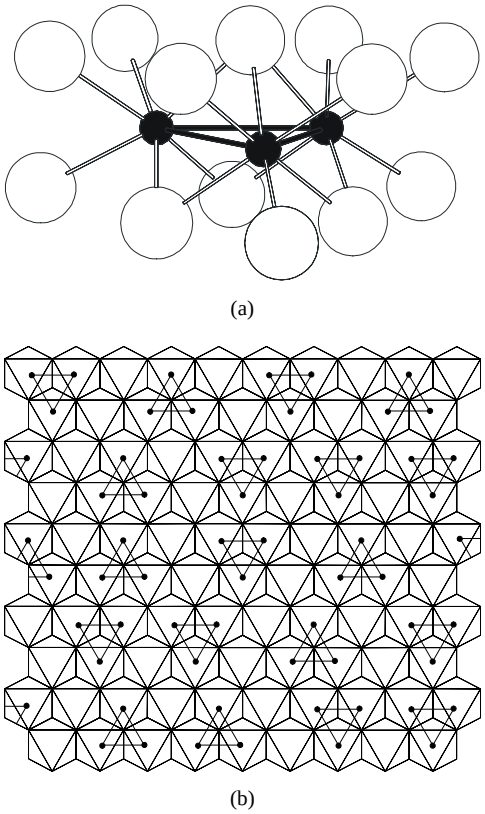

(a)

(b)

Figure 5. (a) The Mo_3O_{13} structural unit (solid circles, Mo; open circles O), (b) Mo–Mo bonded triangles in the $Mo_{2/3}O_2$ layers in Li_2MoO_3 (solid circles, Mo; lithium atoms are omitted for clarity).

useful application of total neutron diffraction data as a check that the crystallographic model used to describe the Bragg diffraction model gives a good description of the local structure. This is important, since determination of the local structure is the goal of most structural studies.

In this case we were able to derive a model which accounts for both the Bragg diffraction and the local structure [17]. This model uses a super-cell of the cell used in the Rietveld refinement, allowing molybdenum and oxygen atoms to be displaced from their average sites to form Mo_3O_{13} clusters. Figure 6 shows that $T(r)$ calculated for this model, which includes the Mo–Mo bonded Mo_3O_{13} units shown in figure 5(a), gives much better agreement, with an R-factor $R_{T(r)} = 0.214$, than is given by the average structure determined using Rietveld refinement (for which $R_{T(r)} = 0.300$). Table 1 shows the difference in the local structure between the average structure, which describes the Bragg diffraction, and the model that includes Mo_3 triangles. Our model gave a similar fit to the Bragg peaks seen in figure 3 as the Rietveld refinement of the average structure, but also predicts extra peaks, which are not seen. These peaks are not observed, because there is no long-range order of the Mo_3O_{13} units within or between the MO_2 layers.

Examination of the contributions from the partial correlation functions to $T(r)$ is revealing. Strong evidence that Mo_3O_{13} units are present comes from the fact that the agreement is now much improved in the regions where O–O correlations are important. This is not the most

Table 1. Selected interatomic distances (Å) in Li_2MoO_3 for the original model describing only the Bragg diffraction and the improved model fitting Bragg diffraction and the local structure seen in $T(r)$.

	Original model fitting Bragg diffraction	Improved model fitting Bragg diffraction and $T(r)$
Mo–Mo		2.585 (×2)
	2.878 (×4 on average)	3.170 (×2 on average)
Mo–O		1.937 (×2)
	2.031 (×6)	1.993 (×1)
		2.052 (×2)
		2.079 (×1)

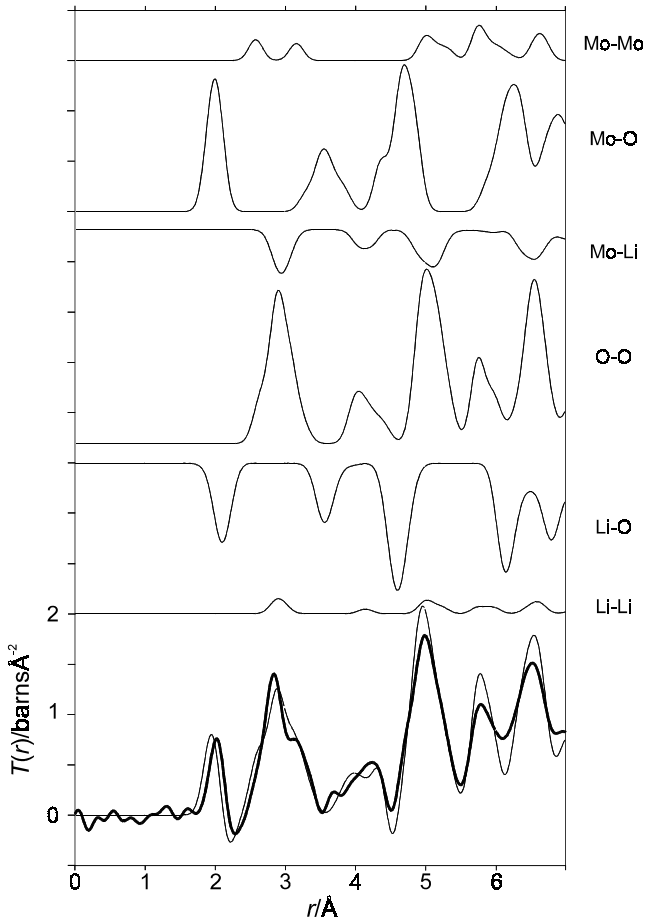

Figure 6. $T(r)_{exp}$ (bold line) and $T(r)_{model}$ (light line) calculated for Li_2MoO_3 for the model containing Mo_3 triangles. The contributions from the partial correlation functions, $t_{ll'}$, are shown.

obvious feature to look for initially, but it clearly reveals that, in order to form Mo_3O_{13} units, the oxygen atoms are displaced from their average positions found in the Rietveld structure. Although Mo–Mo correlations make a relatively small contribution to $T(r)$, the splitting of the Mo–Mo distances into two sets improves the agreement for $T(r)$, on both sides of the peak

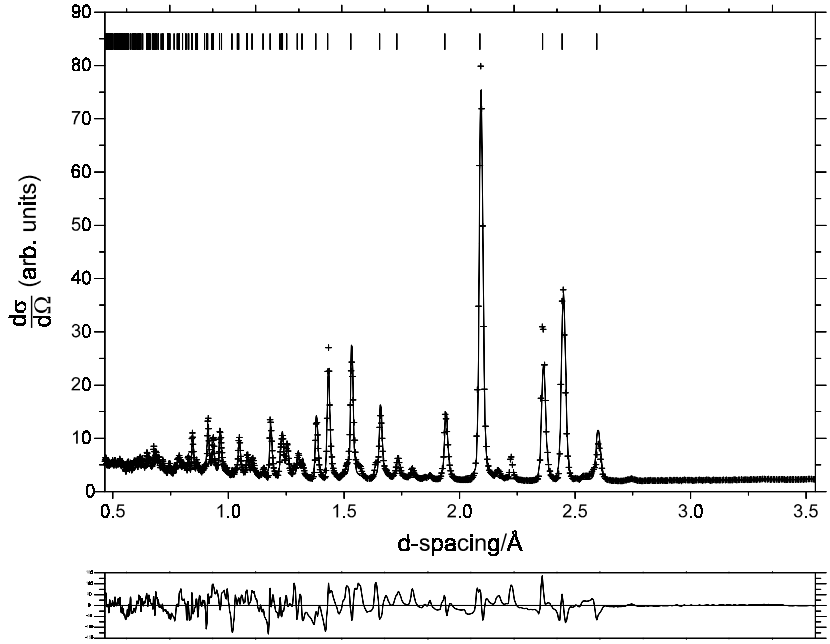

Figure 7. A neutron diffraction profile refinement of $LiMoO_2$ for an incorrect model with six equal Mo–Mo distances. Observed data are indicated by crosses and calculated data by a solid line. Marks directly above the pattern indicate the positions of reflections. A difference curve appears at the bottom. An impurity peak due to Mo metal is present at $d \sim 2.2$ Å.

just below 3 Å. This is especially noticeable around 3.1 Å, where there is a feature in $T(r)$ which is now explained. It appears from an examination of the peak in $T(r)$ at 2 Å that the Mo–O correlations have not been modelled well (see figure 6). However, this is misleading and in fact the problem with modelling the first peak in $T(r)$ arises from the poor description of lithium positions in our super-cell model. The fact that around 2 Å the Mo–O correlations make a positive contribution to $T(r)$ and Li–O correlations a negative contribution means that the behaviour of $T(r)$ in this region is exquisitely sensitive to small lithium displacements from the idealised sites we have placed them on. We expect the lithium atoms to be displaced from these sites, with the lithium atoms moving to satisfy the local bonding requirements of oxygen atoms in this disordered material. A further step in the modelling of the structure of Li_2MoO_3 would be to include such displacements.

Our results show the power of using a combination of structural techniques (Bragg diffraction, total diffraction and EXAFS), rather than modelling the results of a single technique in isolation. In this way, we have successfully determined the structure of the Mo–O units in Li_2MoO_3. Crucial to this work has been the high sensitivity of $T(r)$ to small movements in atomic positions.

We can now explain the disorder in the lithium molybdate, Li_2MoO_3. With the stoichiometry of this material, it is impossible to place Mo_3 units in an $Mo_{2/3}Li_{1/3}$ layer in an ordered fashion, as is shown pictorially by figure 5(b). Thus the disorder is a necessary consequence of the chemical composition of this material and its structure.

3.1.2. The structure of the lithium molybdate $LiMoO_2$. Figure 7 shows the results of the Rietveld refinement for $LiMoO_2$, using data collected on LAD, and the structural model of

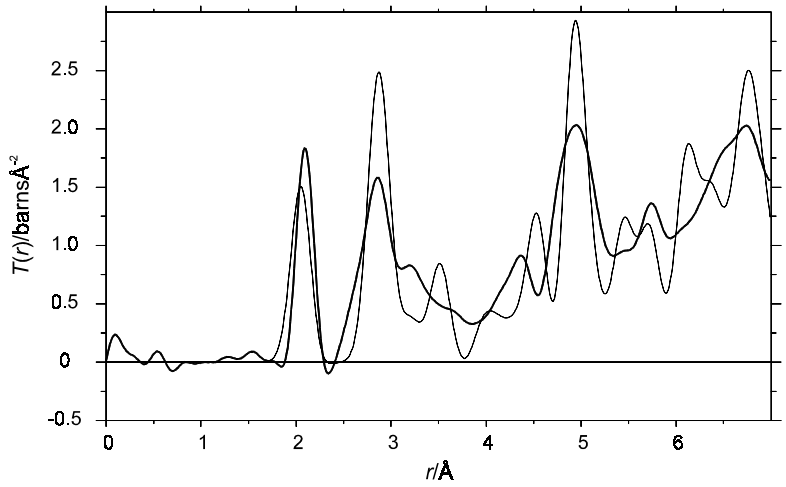

Figure 8. $T(r)_{exp}$ (bold line) and $T(r)_{model}$ calculated for the average incorrect structure with six equal Mo–Mo distances from Rietveld refinement of $LiMoO_2$ (light line). $T(r)$ calculated from the Rietveld model for $LiMoO_2$.

Aleandri and McCarley [15], which is in the space group $R\bar{3}m$. The Rietveld fit, shown in figure 7, although not of the highest quality ($R_{wp} = 0.1212$) looks reasonable and the results of Aleandri and McCarley using this model were considered to be of sufficient quality to be published [15]. However, once again the Rietveld model is seen to be inadequate when the calculated $T(r)_{model}$ is compared with $T(r)_{exp}$. Figure 8 shows the comparison between these two functions, for which the R-factor is calculated to be 0.378 over the region from 1.5 to 7 Å.

In this case we were able, by examining related materials, to produce an ordered model in the space group $C2/m$ which gave a slightly improved fit to the Bragg diffraction ($R_{wp} = 0.0963$, see figure 9) and a dramatically improved fit to $T(r)_{exp}$ ($R_{T(r)} = 0.122$, see figure 10). Table 2 illustrates the differences between the $C2/m$ and $R\bar{3}m$ models. Unlike the $R\bar{3}m$ model, the $C2/m$ model includes Mo–Mo bonded chains, as shown in figure 11. In the fully ordered $C2/m$ model, Mo–Mo bonded chains run along only one crystallographic direction b. In the light of this model, it is easy to see how the disorder arises by a random variation in the chain direction between three equivalent directions in different MoO_2 layers. This variation produces a rhombohedral structure on average, rather than monoclinic structure, figure 11. Thus the disorder in this layered material is due to stacking faults. Careful inspection of figure 9 reveals that the extra reflections predicted by the model in space group $C2/m$ are broad, in agreement with this interpretation. This type of disorder can easily obscure the true structure of the individual layers. The stacking faults occur easily, because the energy difference between the differently orientated layers will be small. A similar effect occurs in simpler structures such as zinc sulphide, ZnS, for which an infinite number of polytypes intermediate between cubic and hexagonal close packing can be formed [18].

3.2. The ion exchange product, D_2MoO_3

The hydrogen molybdenum oxide, H_2MoO_3, and its deuterated form, D_2MoO_3, are poorly crystalline solids prepared from Li_2MoO_3 by ion exchange;

$$Li_2MoO_3 + 2H^+ = H_2MoO_3 + 2Li^+. \tag{11}$$

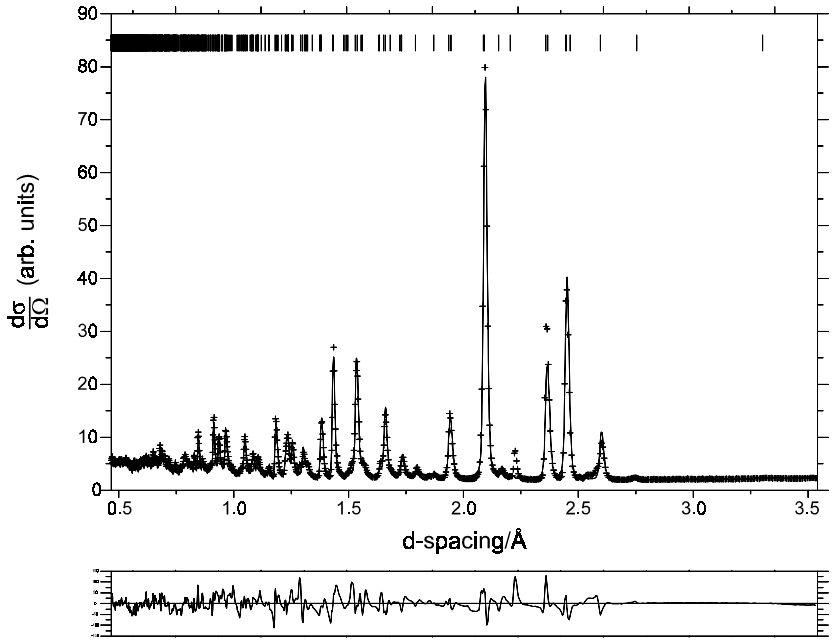

Figure 9. A neutron diffraction profile refinement of $LiMoO_2$, using the correct model containing Mo–Mo bonded chains. Observed data are indicated by crosses and calculated data by a solid line. Marks directly above the pattern indicate the positions of reflections. A difference curve appears at the bottom.

Table 2. Selected interatomic distances (Å) $LiMoO_2$. Table of distances for average and local models. Mo–Mo and Mo–O.

	$R\bar{3}m$ model	$C2/m$ model
Mo–Mo		2.617 (×2)
	2.865 (×6)	2.863 (×2)
		3.122 (×2)
Mo–O(1)		2.056
	2.135 (×6)	2.078 (×2)
Mo–O(2)		2.094 (×2)
		2.102

Gopalakrishnan and Bhat [19] suggested that H_2MoO_3 had a layer structure closely related to that of Li_2MoO_3 because the basal spacing determined from the d-spacing of the first reflection changed only slightly on reaction. The poor crystallinity of H_2MoO_3 makes its structure determination difficult. However, by building upon the results for Li_2MoO_3, we have been able to successfully determine the local structure in this material.

In the diffraction pattern for D_2MoO_3 the Bragg peaks are extremely broad, because of its poor crystallinity, and in addition the peak widths show a hkl dependence. This is clear even in the interference function, $Qi(Q)$, shown in figure 12. To simplify the problem we initially modelled the powder x-ray diffraction pattern for H_2MoO_3 (see figure 13) because the scattering from hydrogen can be ignored, and only Mo and O need to be considered. The 003 peak (at $2\theta \sim 18^\circ$) dominates the pattern, showing that there is good order in the interlayer spacing. Excluding the intense 003 peak from consideration, we began with

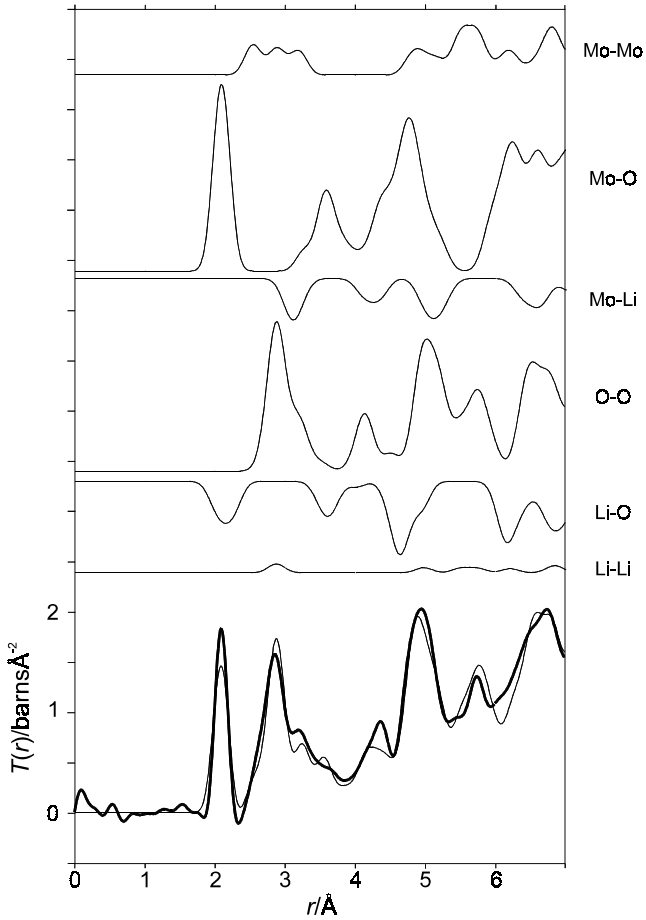

Figure 10. $T(r)_{exp}$ (bold line) and $T(r)$ (light line) calculated for the correct $LiMoO_2$ model containing Mo–Mo bonded chains. The contributions from the partial correlation functions, $t_{ll'}(r)$, are shown.

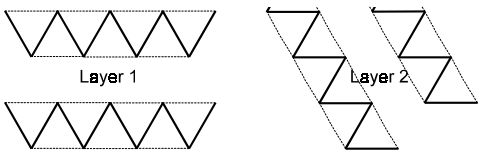

Figure 11. Disorder arising by the Mo–Mo bonded chain direction varying between two of the three equivalent directions in different MoO_2 layers in $LiMoO_2$.

the average structure of Li_2MoO_3 as the starting model. Simple trial and error variation of the oxygen z-parameter produced good agreement between the simulated pattern and the observed intensities for H_2MoO_3 when $z = 0.09$. The simulated powder pattern is shown in figure 13, and the final parameters for molybdenum and oxygen are given in table 3. Modelling the x-ray Bragg intensities shows that the $Mo_{2/3}O_2$ layers remained intact, but are shifted to allow strong hydrogen bonds to form between oxygen atoms in adjacent layers. Figure 14 shows how the layers shift relative to one another and also shows possible hydrogen

Table 3. Structural parameters for H_2MoO_3 in space group $R\bar{3}m$.

Atom	Site	x	y	z
Mo[a]	3b	0	0	1/2
O	6c	0	0	0.09

Lattice parameters: $a = 2.910$ Å, $c = 14.985$ Å.
[a] 2/3 occupancy.

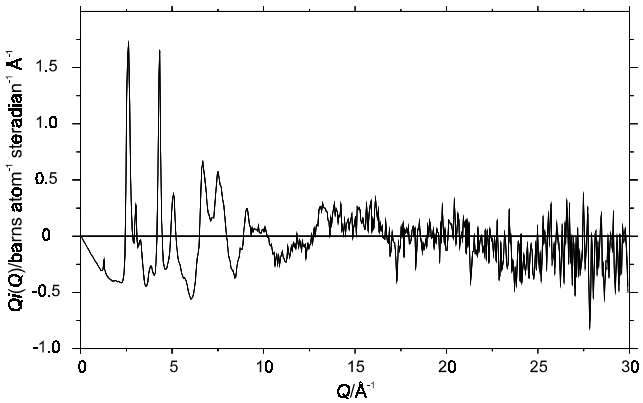

Figure 12. The interference function, $Qi(Q)$, for D_2MoO_3.

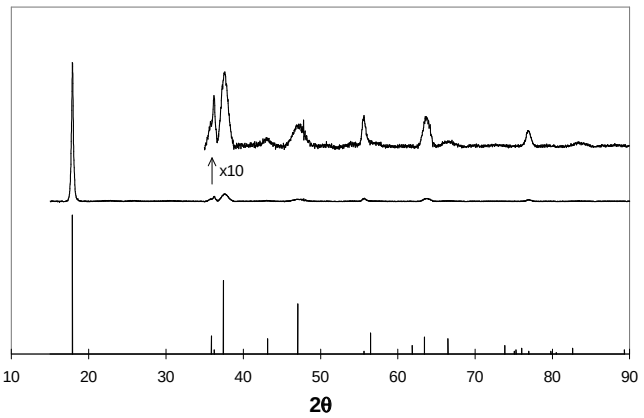

Figure 13. The powder x-ray diffraction pattern (top two curves), measured with a wavelength 1.5405 Å, and the simulated pattern (bottom) of H_2MoO_3.

positions (note only one of each pair of hydrogen atom positions shown can be occupied at one time).

We then used total neutron diffraction to reveal the local structure in D_2MoO_3, as shown by $T(r)_{exp}$ in figure 15. To model the correlation function, we used a similar procedure to that adopted for Li_2MoO_3. We first constructed a super-cell that allowed us to move molybdenum atoms off the average sites found in the model given in table 3 to form metal–metal bonded Mo_3O_{13} units. Then deuterium atoms were added to the model to give reasonable O–D and D $\cdots$ O distances (another advantage of the super-cell is that it allowed us to produce a model with fully occupied deuterium positions without the problem of close deuteron contacts seen

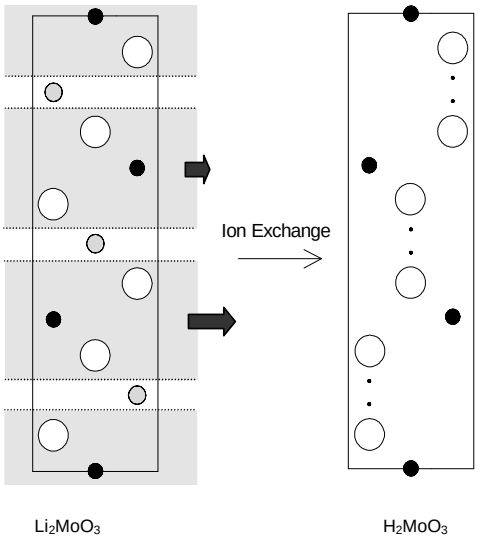

Figure 14. The change in stacking sequence during the ion-exchange reaction, Li_2MoO_3 to H_2MoO_3 (solid circles, Mo/Li ($Mo_{2/3}Li_{1/3}$ in Li_2MoO_3 and $Mo_{2/3}$ in H_2MoO_3); open circles, O; shaded circles, Li; small solid circles, H). MO_2 layers in Li_2MoO_3 are indicated by light shading, and their relative movements on ion exchange by the bold arrows.

Table 4. Atomic parameters used to calculate $T(r)$ for $D_{3/2}MoO_3$.

Atom	Site	x	y	z
Mo[a]	9b	0.1898	0.8102	0.1679
O(1)	3a	0	0	0.4076
O(2)	3a	0	0	0.2364
O(3)	9b	0.8454	0.1546	0.0993
O(4)	9b	0.4941	0.5059	0.2430
D(1)	9b	0.8454	0.1546	0.0310
D(2)	3a	0.3333	0.6667	0.9667

Space group $R\bar{3}m$, lattice parameters: $a = 5.820$ Å, $c = 14.985$ Å.
[a] 8/9 occupancy.

Table 5. Selected interatomic distances (Å) in $D_{3/2}MoO_3$.

Mo–O(1)	2.016	O(3)–D(1)	1.024
Mo–O(2)	2.171	D(1)–O(4)	1.827
Mo–O(3)	2.041 × 2	O(2)–D(2)	0.953
Mo–O(4)	1.908 × 2	D(2)–O(1)	1.612
Mo–Mo	2.506		

in figure 14). After adding deuterons to form O–D $\cdots$ O linkages between the layers, we have produced a model with the stoichiometry $D_{3/2}MoO_3$. Table 4 gives the final parameters of our model, and both $T(r)_{model}$ and $T(r)_{exp}$ are shown in figure 15. Selected interatomic distances for this model are given in table 5. There is good agreement between $T(r)_{model}$ for $D_{1.5}MoO_3$ and $T(r)_{exp}$ for D_2MoO_3. The calculated $T(r)_{model}$ fits the general features of $T(r)_{exp}$, but it is too ordered, as should be expected, since a fully ordered model is being used to describe a very disordered crystalline material.

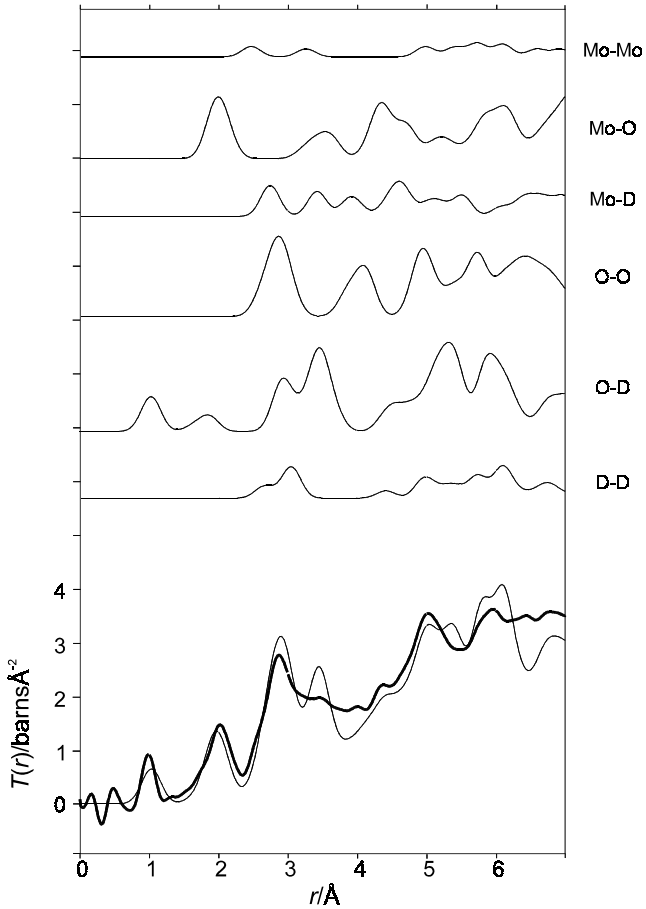

Figure 15. $T(r)_{exp}$ (bold line) and $T(r)$ (light line) calculated for $D_{3/2}MoO_3$ from the parameters in table 4. The contributions from the partial correlation functions, $t_{ll'}$, are shown.

Clearly another problem remains: where are the missing deuterons? Figure 16 shows the structure produced by our model and also reveals one of the problems remaining in our modelling: that there are no sites left for additional deuterons! There is a solution, which is not apparent in the structural diagram. In figure 16 all the Mo sites are shown as occupied, despite the fact that the occupancy is 8/9 (see table 4). We have allowed for this partial occupancy when calculating $T(r)$, but not when building the structural model. The partial occupancy of Mo sites means that one Mo_3 unit in nine is missing from the fully occupied structure shown in figure 16. This allows the possibility of forming OD_2 groups coordinated to molybdenum around these vacancies, and also the removal of some of the oxygen atoms, as free D_2O.

The structure of D_2MoO_3 is indeed more complicated than that of Li_2MoO_3. Combining the results of Bragg diffraction and total neutron diffraction has allowed us to determine that the basic layer structure of Li_2MoO_3 is retained on ion exchange, that the $Mo_{2/3}O_2$ layers shift to allow hydrogen bonds between the layers, and that the Mo_3O_{13} metal–metal bonded structural units remain intact. The last point is very important as it explains why this form of H_2MoO_3 is stable to aerial oxidation.

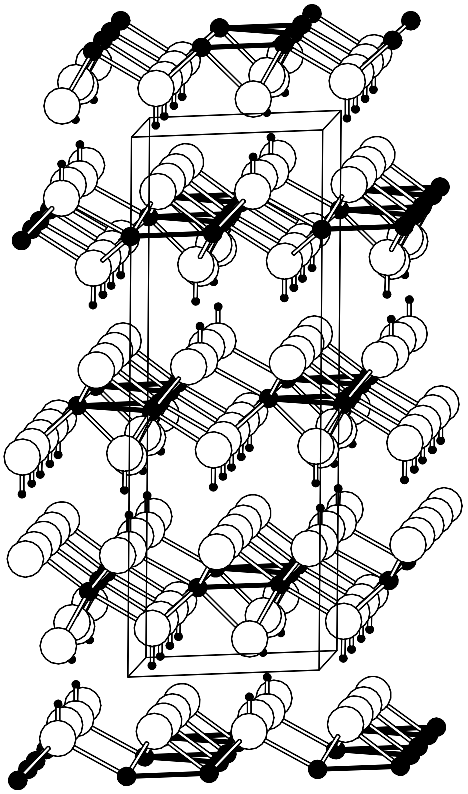

Figure 16. Structural model for $D_{3/2}MoO_3$ (solid circles, Mo; open circles, O; small solid circles, D).

4. Other materials

The materials discussed above all have layer structures. However, the approach we discuss has more general applicability, for example in the structural study of colossal magnetoresistive materials, which have strong three-dimensional connectivity. These materials are intrinsically disordered because of their chemical stoichiometry. We omit any further discussion here because we report our results on these materials elsewhere in this volume [20].

Recently we applied the methodology described above to a more complicated structural problem, the disordered crystalline molybdate $LaMo_2O_5$ [21]. This oxide contains two unusual Mo–Mo bonded units, an octahedral Mo_6O_{18} cluster and a new type of Mo–Mo bonded sheet. In the average structure found from Bragg scattering [22] two-thirds of the sites had 50% occupancy. We were able to produce models that proved that the Mo–Mo bonded units were indeed present in the local structure, by modelling $T(r)$, and were compatible with the average structure found in the Rietveld refinement. A full description of this work can be found elsewhere [21].

5. Conclusion and future prospects

The case studies described above illustrate how total neutron diffraction studies, in which both the Bragg diffraction and the derived correlation functions are modelled, can yield new insights

into the structures of disordered crystalline materials. LAD has been invaluable in providing us with the data required to commence this type of study. We look forward to pursuing this work using the new General Materials Diffractometer, GEM [9], at the ISIS spallation neutron source. GEM will have improved resolution in reciprocal space ($\Delta d/d = 0.2\%$). This will allow the study of more complicated structures, with larger unit cells, and give improved determination of the average structure. The large number of detectors will yield $Qi(Q)$ with better statistical accuracy and, together with the more stable detectors, more accurate $T(r)$ determinations. The improved statistical accuracy also offers the prospect of being able to attain higher values of Q and hence to achieve better real-space resolution.

References

[1] Dove M T, Keen D, Hannon A C and Swainson I P 1997 *Phys. Chem. Miner.* **24** 311–7
[2] Keen D A 1998 *Local Structure from Diffraction* ed S J L Billinge and M F Thorpe (New York: Plenum) pp 101–19
[3] Keen D A and Dove M T 1999 *J. Phys.: Condens. Matter* **11** 9263–73
[4] Soper A K, David W I F, Sivia D S, Dennis T J S, Hare J and Prassides K 1992 *J. Phys.: Condens. Matter* **4** 6087–94
[5] Dmowksi W, Toby B H, Egami T, Subramanian M A, Gopalakrishnan J and Sleight A W 1988 *Phys. Rev. Lett.* **61** 2608–11
[6] Teslic S, Egami T and Velhand D 1997 *J. Phys. Chem. Solids* **57** 1537
[7] Louca D, Egami T, Brosha E L, Röder H and Bishop A R 1997 *Phys. Rev.* B **56** 8475–8
[8] Mellergård A and McGreevy R L 1997 *Physica* B **234–236** 713–4
[9] Hannon A C 1999 *Encyclopedia of Spectroscopy and Spectrometry* ed J Lindon, G Tranter and J Holmes (London: Academic) at press
[10] Hannon A C 1999 *Encyclopedia of Spectroscopy and Spectrometry* ed J Lindon, G Tranter and J Holmes (London: Academic) at press
[11] Lorch E 1969 *J. Phys. C: Solid State Phys.* **2** 229–37
[12] Hannon A C, Grimley D I, Hulme R A, Wright A C and Sinclair R N 1994 *J. Non-Cryst. Solids* **177** 299–316
[13] Young R A (ed) 1993 *The Rietveld Method (International Union of Crystallography Monographs on Crystallography 5)* (Oxford: Oxford University Press)
[14] James A C W P and Goodenough J B 1988 *J. Solid State Chem.* **76** 87–96
[15] Aleandri L E and McCarley R E 1988 *Inorg. Chem.* **27** 1041–4
[16] Hibble S J and Fawcett I D 1995 *Inorg. Chem.* **34** 500–8
[17] Hibble S J, Fawcett I D and Hannon A C 1997 *Acta Crystallogr.* B **53** 604–12
[18] Hyde B G and Andersson S 1989 *Inorganic Crystal Structures* (New York: Wiley) pp 55–6
[19] Gopalakrishnan J and Bhat V 1987 *Mater. Res. Bull.* **22** 769–74
[20] Hibble S J, Cooper S P, Hannon A C, Fawcett I D and Greenblatt M 1999 *J. Phys.: Condens. Matter* **11** 9221–38
[21] Hibble S J, Cooper S P, Hannon A C and Patat S *Acta Crystallogr.* B **55** 683–97
[22] Hibble S J, Cooper S P, Hannon A C, Patat S and McCarroll W H 1998 *Inorg. Chem.* **37** 6839–46